

Comparison of wavelet estimates from VSP and surface data

Linping Dong, Gary F. Margrave, and Kevin W. Hall

ABSTRACT

The wavelets measured in VSP downgoing waves are extracted at arrival time of the first break in the VSP data, and then convolved with a time-frequency domain constant-Q filter. The filtered wavelets obtained from VSP are compared to the propagating wavelet estimated from surface data by Wiener, frequency domain spiking and Gabor deconvolutions. To verify the accuracy of the results from surface data, we use normalized cross-correlation to carry out the comparison. This study shows that wavelet estimates from VSP surveys can be used to evaluate the accuracy of the wavelets estimated from surface data. Our results are consistent with the hypothesis that Gabor deconvolution can accurately estimate the nonstationary wavelets embedded in real seismic records. These results also suggest that Gabor deconvolution is superior to a multi-window Wiener or frequency domain spiking deconvolution.

INTRODUCTION

The accuracy of wavelets estimated by deconvolution of surface seismic data can be verified by several approaches. Traditionally, the results of deconvolution are compared to synthetic seismograms generated from sonic logs. If these results are consistent in time and amplitude, the wavelet estimates are considered to be accurate. In most cases this comparison is difficult because the software used to generate synthetics typically convolves the reflection coefficients with a stationary wavelet. Here, we compare the wavelet estimates from VSP downgoing waves with wavelet estimates from deconvolution of surface data. The wavelets obtained from VSP downgoing waves are direct measurements of the propagating wavelets. However, there are important differences between wavelet estimates from VSP and surface data because the ray paths are different.

A simultaneous VSP and 2D surface seismic survey was provided by EnCana (formerly PanCanadian) for this research. The recording geometry is shown in Figure 1. Receivers were positioned between 322 and 1820 m depth at a receiver interval of 20 m for a total of 75 receiver locations within the borehole. An additional 78 geophones were placed on the surface between 30 and 2310 m from the borehole at a 30 m interval. Five vib points were used for this survey, located 27, 430, 960, 1350, and 1700 m from the borehole. A 12 s, 10-96 Hz non-linear sweep was used to record 16 second uncorrelated shot records at a 2 ms sample rate.

PROPAGATING WAVELET ESTIMATION

The propagating wavelet is closely related to nonstationarity of wavelets. Wavelet nonstationarity is the time-variant change in waveform, that is primarily the result of the effects of wavefront divergence and frequency attenuation (Yilmaz, 1987). The wavefront divergence can be easily corrected if we know the velocity of wavelet propagation. Suppose the effect of geometric spreading on the wavelets has been

removed, the propagating wavelet can now be modelled as an attenuated source signature which can be expressed as

$$\omega_p(t, f) = \omega(f)\alpha_Q(t, f) \quad (1)$$

where $\omega_p(t, f)$ denotes the propagating wavelet and $\omega(f)$ is the spectrum of the stationary source signature (Margrave and Lamoureux, 2001). In our case, the surface and VSP data have the same source. The source signature, obtained by auto-correlating the vibroseis sweep and its amplitude spectrum are shown in Figure 2. The attenuation term, $\alpha_Q(t, f)$, can be written as:

$$\alpha_Q(t, f) = e^{-\frac{\pi ft}{Q} + iH\left(\frac{\pi ft}{Q}\right)}, \quad (2)$$

where H denotes the Hilbert transform and Q is the non-frequency-dependent quality factor (Aki and Richards, 1980). Equation 2 shows the attenuation surface is a minimum-phase, time-variant low-pass filter.

Wavelet estimation from VSP data

Downgoing waves recorded on VSPs represent a direct observation of the propagating wavelet. Major steps in VSP wavelet estimation are: 1) vertical sum; 2) geometric spreading correction; 3) downgoing wave flattening; and 4) f-k filter. The purpose of the vertical sum is to improve the S/N ratio. The geometric spreading correction removes nonstationarity relating to wavefront divergence which is independent of frequency. The velocity function used in the geometric spreading correction should be the same as used for surface seismic processing (next section). After flattening downgoing waves, a f-k filter is applied to separate the downgoing waves from the full wavefield.

Figure 3 shows the vertical component VSP record used in this study, after vertical summation. Figure 4 shows the same record after separation of the downgoing wave field, and Figure 5 shows the resulting 1D-FFT amplitude spectra. The phenomenon that high-frequency components decay with increasing time can be easily observed from the wavelets and their spectra extracted at 0.25, 0.47, and 0.66s (Figure 6). To examine the phase property of the wavelets, minimum-phase spiking deconvolution is applied to the results shown in Figure 4. If the deconvolved result is a spike the signal is said to be minimum phase. Figures 7 and 8 show the spiking deconvolved downgoing waves and their amplitude spectra which are similar to spikes. Therefore, we believe the propagating wavelet seen on the VSP data is likely minimum-phase.

Wavelet estimation from surface data

For deconvolution of surface data, the wavelets are extracted by statistical approaches. Commonly used deconvolution methods, such as Wiener and frequency domain spiking deconvolution (FDSD), require the assumptions of minimum phase, stationarity, and random (white) reflectivity. Usually nonstationarity is reduced before deconvolution by applying a geometric spreading correction, and possibly

inverse- Q filtering. Therefore, we cannot extract the propagating wavelet after inverse- Q filtering. This problem can be partly solved by using multi-window stationary deconvolution such as Wiener and FDSO. A more sophisticated approach for propagating wavelet estimation was proposed by Margrave and Lamoureux (2001). A propagating wavelet was estimated via a Gabor spectral model by Grossman et al. (2002). The propagating wavelet can be extracted directly by performing a Gabor transform, smoothing the resulting spectrum, and then doing an inverse Gabor transform. Figure 9 shows the processing flow applied to surface data prior to wavelet estimation by Gabor transform.

The shot records contain ground roll and air waves, particularly at near offsets, which will affect the wavelet estimation (Figure 10). Low frequency and low velocity noise was suppressed with the ProMAX surface-wave attenuation module. This module attempts to remove linear noise with f-k filters. After noise suppression, it can be seen that S/N has been improved on the shot gather (Figure 11).

After pre-processing, the next step is to choose traces with high S/N from surface data (green box, Figure 11), and select time windows corresponding to the first arrival times of the downgoing wave field in the VSP data. To maintain consistency with VSP downgoing waves, we try to estimate wavelets from the same depth. The relationship between the one-way traveltime to a receiver in the borehole on an offset VSP (t_1), and two-way traveltime of a reflection recorded at the surface from a reflector at the same depth as the receiver in the borehole (t_2), can be expressed as

$$t_2 = \sqrt{\frac{x^2}{v_{stk}^2} + 4 \left(\frac{t_1^2 v_a^2 - c^2}{v_{stk}^2} \right)}, \quad (3)$$

where v_a is the average velocity at time, t_1 ; v_{stk} is the stacking velocity estimated from the surface seismic; c is the horizontal distance between shot location and borehole, and x is the source-receiver offset at the surface. From the stack section shown in Figure 12, nearly all the events above 2 seconds are horizontal, and there is little lateral variation in the stacking velocity. So, it is reasonable to use Equation 3 in this case. Here, t_1 is measured directly from downgoing wavefield in the VSP data, v_a is calculated from t_1 , and the depth of the receiver in the borehole, c , is equal to 27 m for the shot gather used, and v_{stk} is estimated from CMP gathers of surface data. The calculated two-way traveltime (t_2) is selected as the window position for the wavelet estimation, for comparison with the wavelet at t_1 from the VSP data. Window length will affect the time-frequency resolution of the propagating wavelet (Margrave and Lamoureux, 2001). It can be chosen by comparing a wavelets from the surface data to Q -filtered wavelets from the VSP data. Here, we select window length equal to 0.2 s for this study.

Three methods were applied to estimate the propagating wavelet from surface data. In Wiener deconvolution, the inverse operator is obtained with the Wiener-Levinson algorithm. The wavelet is actually a match filter, for matching the inverse operator to an impulse. In FDSO, the amplitude spectrum of the windowed data is smoothed with a boxcar 5 Hz width, and stabilized with a factor of 0.001 to get the amplitude spectrum of the wavelet, followed by a Hilbert transform to calculate the phase spectrum. Finally, the wavelet is reconstructed by inverse Fourier transforming the estimated spectra. To estimate wavelets with Gabor deconvolution, we Gabor-transform data in Gaussian windows with 80 percent window overlap, then use a hyperbolic operator to smooth the time-variant amplitude spectrum to obtain the amplitude spectrum of the propagating wavelet. Then we extract the amplitude spectrum of the wavelets at time, t_2 , (Equation 3) and reconstruct the wavelets with the Hilbert transform. Figure 13 show the wavelets estimated at 0.5, 0.8, and 1.1 s using these deconvolution methods. Figures 14 display the amplitude spectra of the wavelets shown in Figure 13. Obviously, the propagating wavelets experiences high-frequency attenuation and dispersion with increasing time. Wavelets and spectra show that the wavelet estimated from Gabor deconvolution is more stable than that obtained from the other two approaches. Note that the amplitude of the propagating wavelet estimated by Wiener deconvolution doesn't decay with increasing time, since the normalized autocorrelation is used in deriving the deconvolution operator.

WAVELET COMPARISON BY Q-FILTER

After applying a geometric spreading correction to the wavelet estimates, we assume the major differences between wavelets from VSP and surface data are caused by attenuation. If we assume the quality factor (Q) is the same for both VSP and surface data, the spectral ratio of the VSP and surface data wavelets can be written as

$$\frac{S_{sur}(t_2, f)}{S_{vsp}(t_1, f)} = e^{-\frac{\pi f(t_2-t_1)}{Q(t_1)} + i\frac{\pi(t_2-t_1)}{Q(t_1)}H(f)}, \quad (4)$$

where $S_{vsp}(t_1, f)$ is the spectrum of the wavelet estimated from VSP data, and $S_{sur}(t_2, f)$ is the spectrum of the wavelet estimated from surface data. From this equation we can approximate $S_{vsp}(t_1, f)$ by $S_{sur}(t_2, f)$ or vice versa. The constant- Q value, $Q(t_1)$, can be estimated from the downgoing wavefield in VSP data. The Q estimate from VSP data is usually more reliable (White 1992). Of many methods available for Q estimation, the spectral ratio approach is more accurate than others in noise-free cases (Tonn. 1991), This can be expressed as

$$\ln\left(\frac{A(t_{02}, f)}{A(t_{01}, f)}\right) = \pi f(t_{02} - t_{01})/Q, \quad (5)$$

where $A(t_{02}, f)$ and $A(t_{01}, f)$ are the amplitude spectra of a propagating wavelet at one-way time t_{02} and t_{01} respectively. f is frequency. The Q value is estimated by linear regression of the log spectral ratio in the frequency domain. In our case, since

the source signature is known (Figure 2), its amplitude spectrum can be used as a reference spectrum, $A(t_{01}, f)$. So, here t_{01} is equal to zero and Q estimated from Equation 5 is actually the average Q from the surface to the depth each geophone is located in the borehole. Figure 15 shows log spectral ratio and Q values estimated for times 0.24, 0.38, 0.53, and 0.63 s using Equation 5. The frequency range selected to estimate Q is the same as the source signature (Figure 2). Figure 16 shows the average Q estimated from the wavelets obtained from the VSP data, and its fitted curve. As a whole, the Q estimates increase with increasing time. A low Q zone between 0.55 and 0.64 s may represent a high absorption area.

Suppose Q is independent of the ray path, and wavelets received at each depth travel back to the surface. This procedure can be simulated with Equation 4. This is equivalent to a time-frequency domain forward- Q filter. The filter shown in Figure 17 was calculated from the time-variant Q function shown in Figure 16. Figure 18 shows the wavelets estimated from surface data compared to the Q -filtered wavelets from the VSP data. At the two-way time of 0.5 s, the Q -filtered VSP wavelet from an equivalent reflector contains higher frequencies. With increasing time, high-frequency components are attenuated and the Q -filtered wavelets gradually conform to the wavelets estimated from surface data. Figure 19 shows the amplitude spectra corresponding to the wavelets in Figure 18. It is apparent that, at greater traveltimes, the propagating wavelet from Gabor deconvolution is the closest match to the Q -filtered wavelet from the VSP.

We apply normalized cross-correlation to compare the wavelets estimated from surface data and Q -filtered wavelets from VSP data. Normalized cross-correlation can be written as

$$Corr(\tau, t) = \frac{\sum_l a(\tau, t+l)b(\tau, l)}{\sqrt{\sum_l a^2(\tau, l)\sum_l b^2(\tau, l)}}, \quad (6)$$

and

$$Maxcorr(\tau) = \max_l (|Corr(\tau, t)|), \quad (7)$$

where a denotes Q -filtered VSP wavelets and, b , the wavelets estimated from surface data. $Corr(\tau, t)$ is the normalized cross-correlation between a and b . $Maxcorr(\tau)$ is the peak value of the cross-correlation at different times, which represents the correlation between two wavelets at time τ . Figure 20 shows the peak curves of cross-correlation from the three deconvolution methods evaluated in this study. The wavelets estimated from Gabor deconvolution are more stable, and most similar to the wavelets from VSP.

DISCUSSION AND CONCLUSIONS

We have shown a possible approach comparing wavelet estimates from VSP and surface data. The comparison result depends upon many factors, such as the consistency between VSP and surface data, accuracy of Q estimates, quality of the data used for wavelet estimation, and accuracy of the deconvolution methods. The most important factor is data quality. Our results are consistent with the hypothesis that Gabor deconvolution can accurately estimate the nonstationary wavelets embedded in real seismic records. These results also suggest that Gabor deconvolution is superior to a multi-window Wiener approach.

ACKNOWLEDGEMENTS

We thank EnCana (formerly PanCanadian) for providing the VSP and surface seismic data and also acknowledge financial support from CREWES, POTSI, MITACS, and NSERC. We thank all of our sponsors for their support.

REFERENCES

- Aki, K. and Richards, P.G., 1980, Quantitative Seismology: Theory and Methods, Vol. 2, W.H. Freeman and Company.
- Grossman, J.P., Margrave, G.F., Lamoureux, M.P., and Aggarwala, R, 2002, Constant-Q wavelet estimation via a Gabor spectral model: 2002 CSEG National Convention.
- Margrave, G.F. and Lamoureux, M.P., 2001, Gabor deconvolution: CREWES Research Report, **13**.
- Tonn, R., 1991, The determination of the seismic quality factor Q from VSP data: a comparison of different computational methods: Geophysical Prospecting, **39**, 1-27.
- White, R.E., 1992, The accuracy of estimating Q from seismic data: Geophysics, **57**, 1508-1511.
- Yilmaz, O., 1987, Seismic Data Processing. Published by SEG.

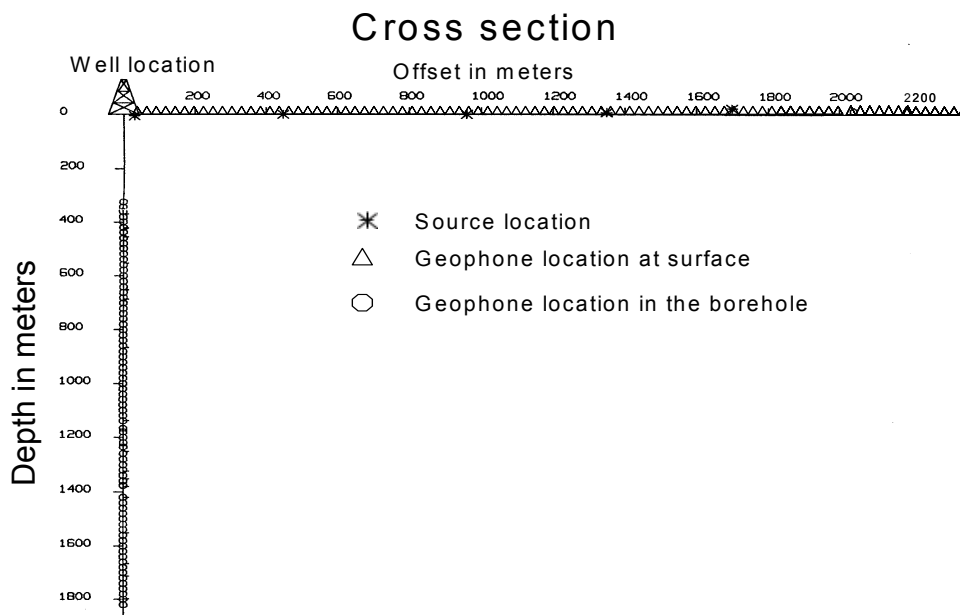


FIG.1: Joint VSP-surface seismic acquisition geometry. There were 75 receiver locations in the well and 78 on the surface. Vibe points were located 27, 432, 960, 1350 and 1700 m from the borehole.

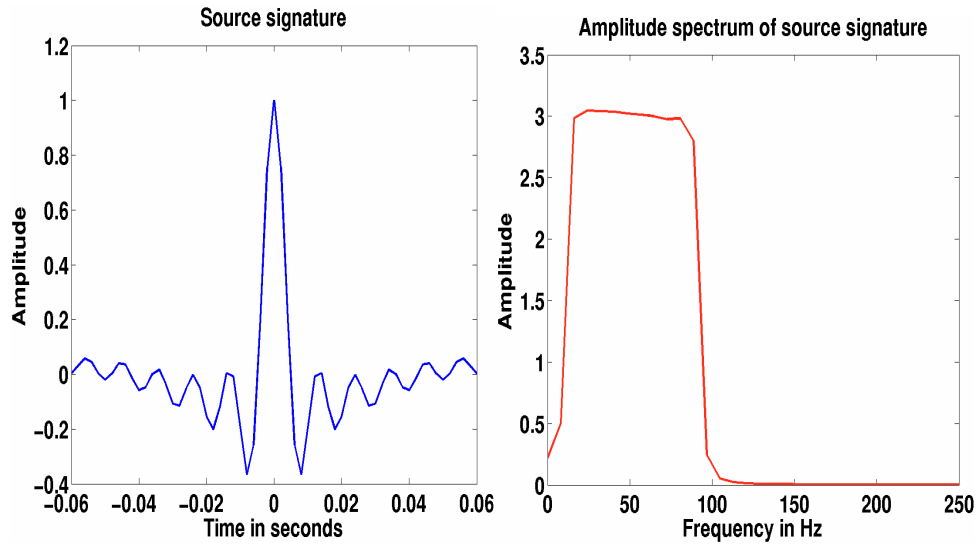


FIG. 2: Source signature (auto-correlation of vibroseis sweep), and its amplitude spectrum.

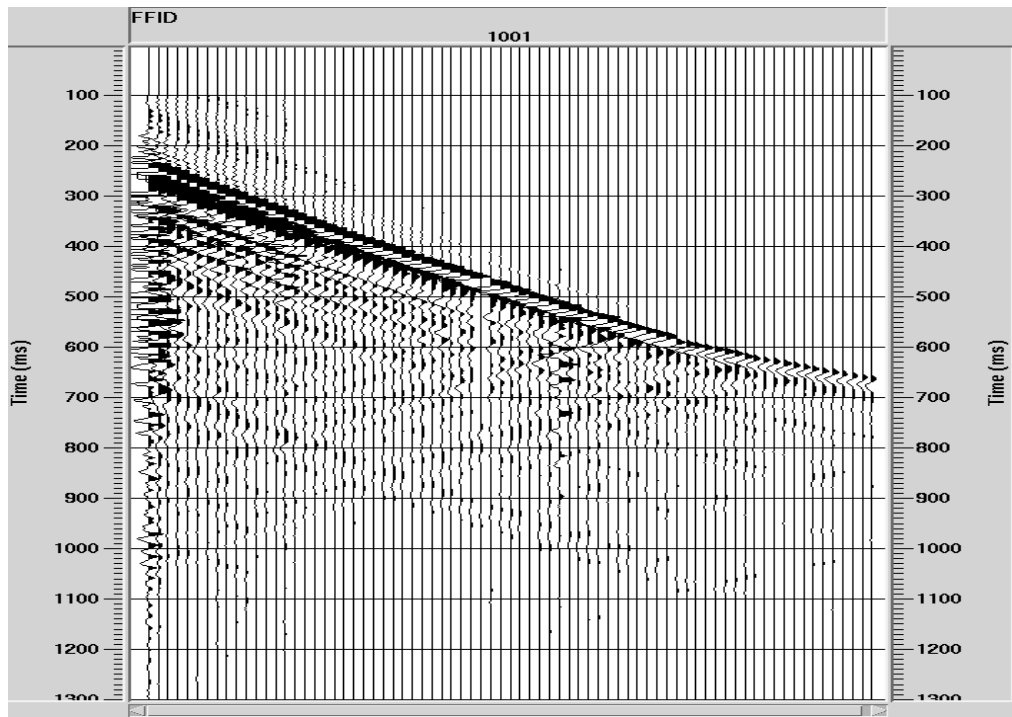


FIG. 3: Vertical component of zero-offset VSP field record after vertical summation.

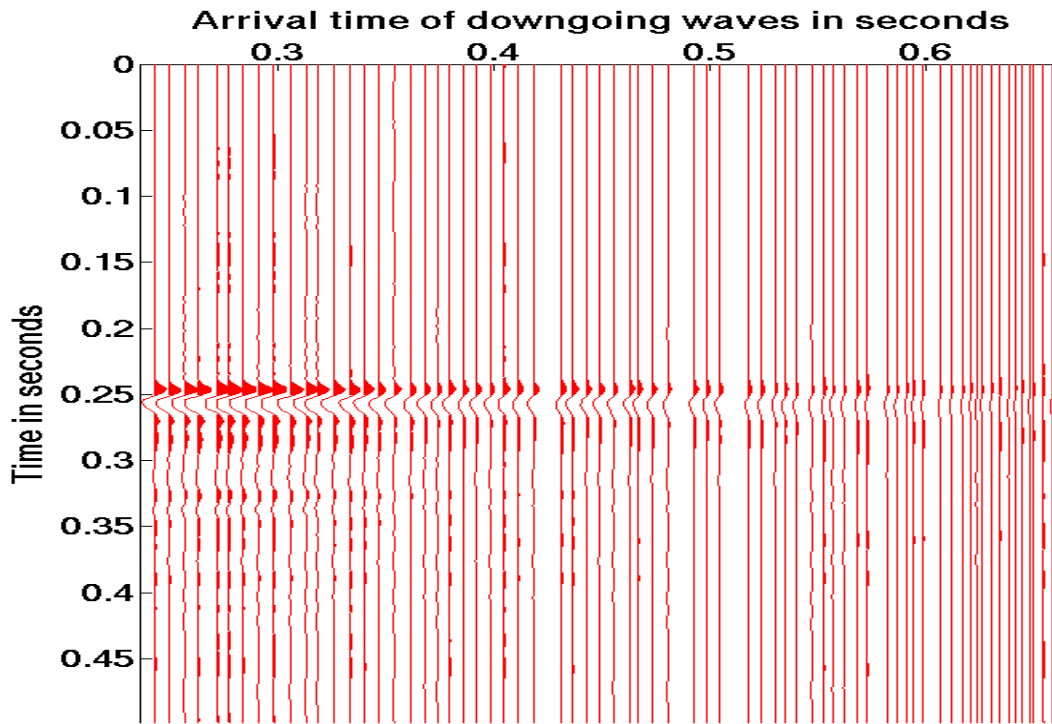


FIG. 4: Downgoing waves from the VSP data.

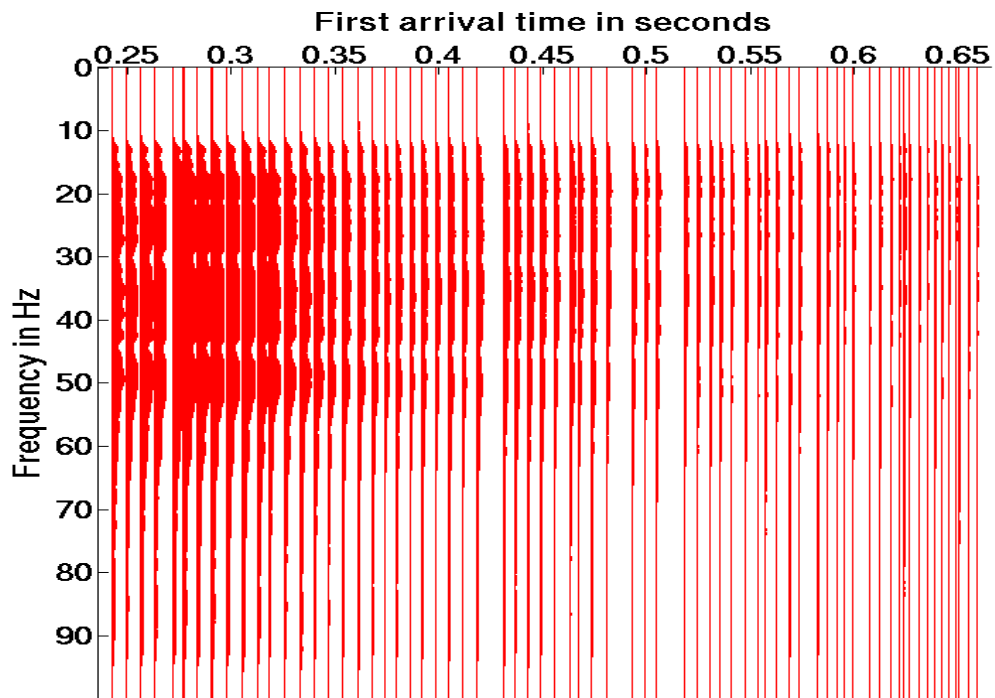


FIG. 5: Amplitude spectra of downgoing waves shown in Figure 4.

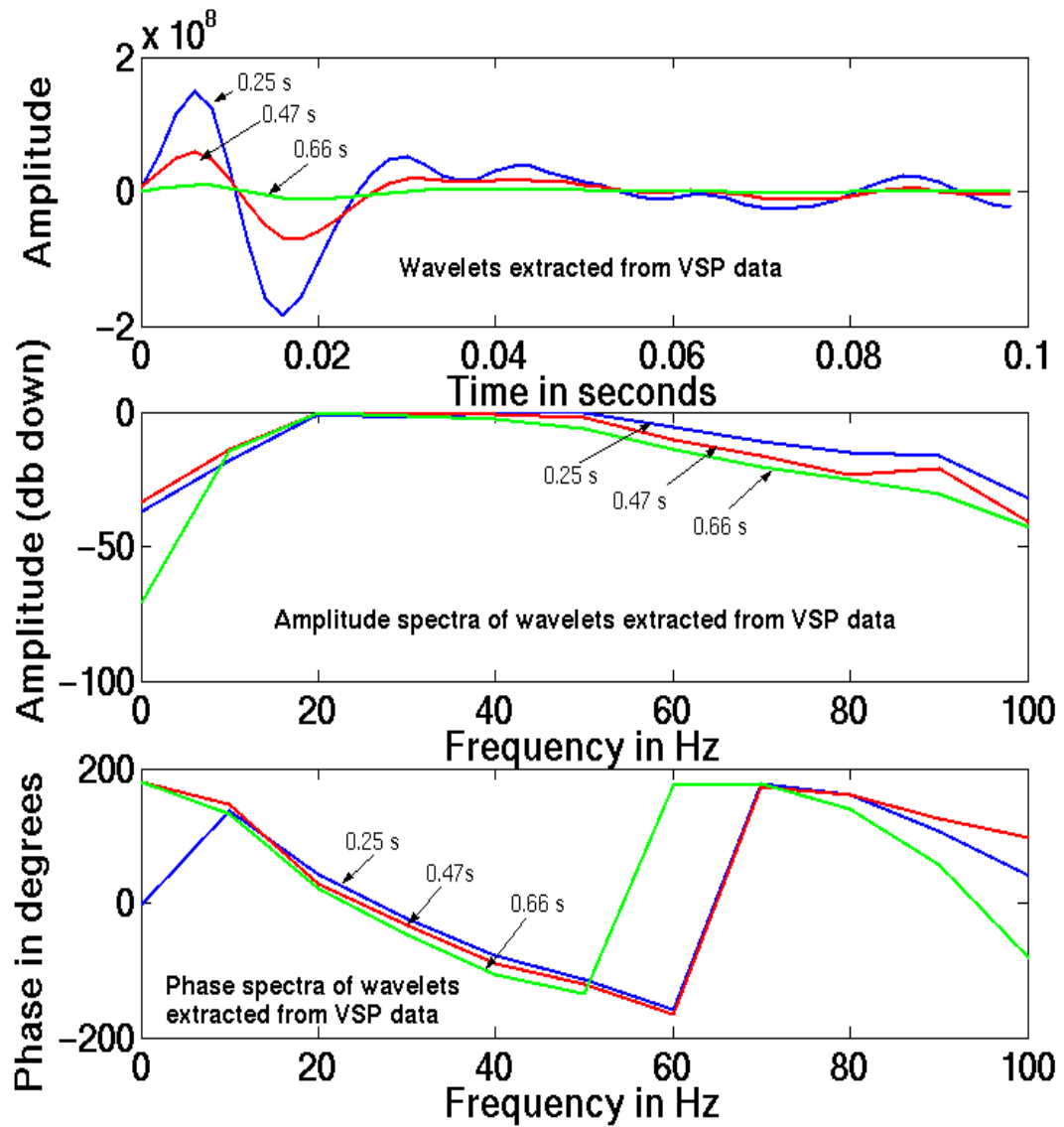


FIG. 6: Wavelets and their spectra (amplitude and phase) extracted from VSP data at 0.25, 0.47, and 0.66 s.

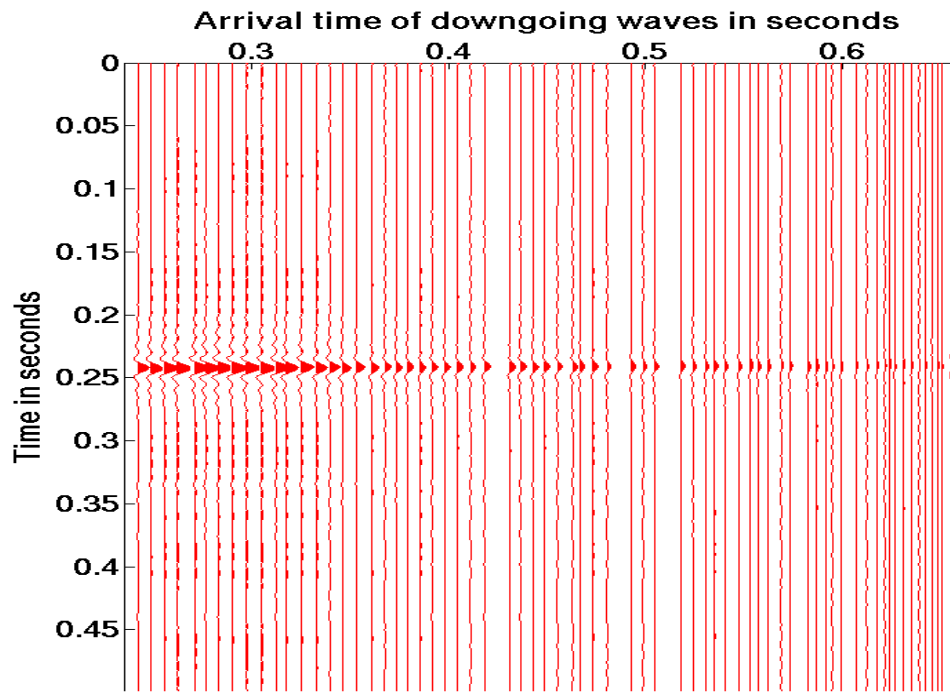


FIG. 7: Deconvolved downgoing waves by Wiener minimum-phase deconvolution.

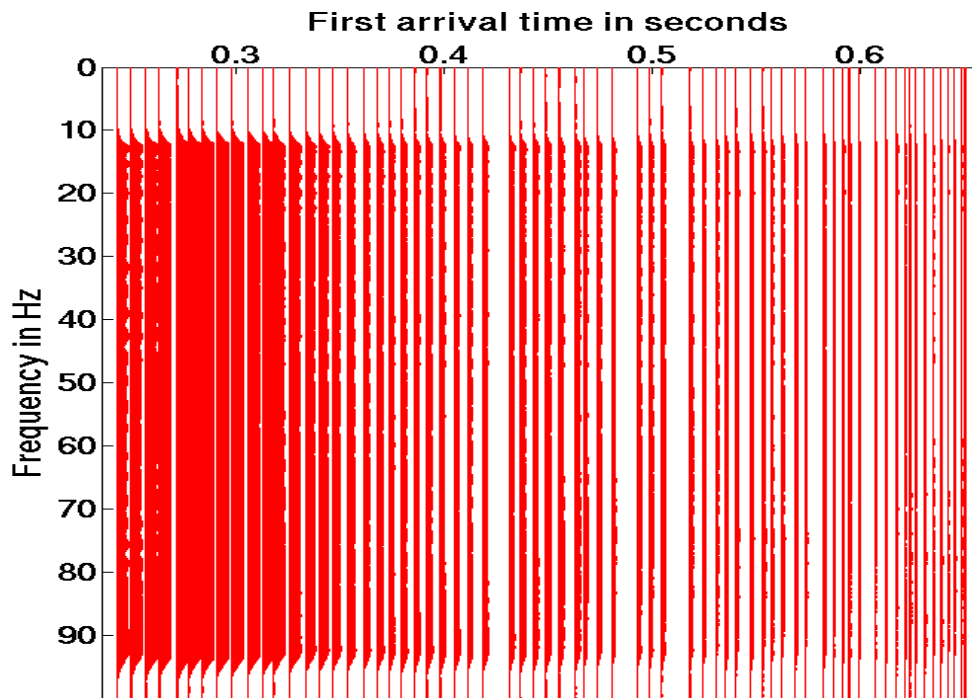


FIG. 8: Amplitude spectra of deconvolved downgoing waves.

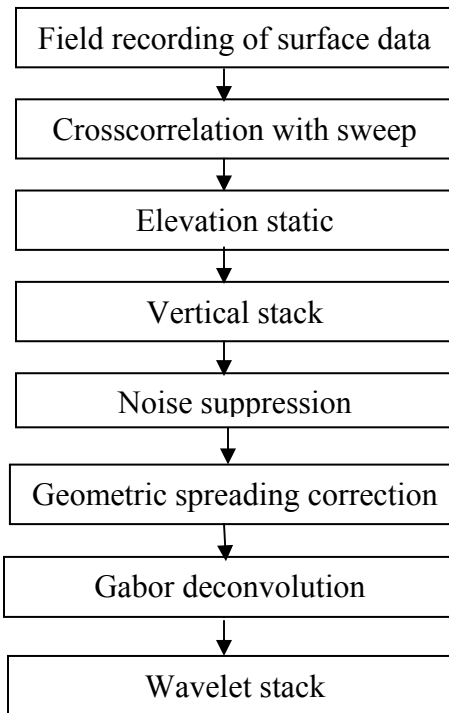


FIG. 9: Flow chart for wavelet estimation from surface data.

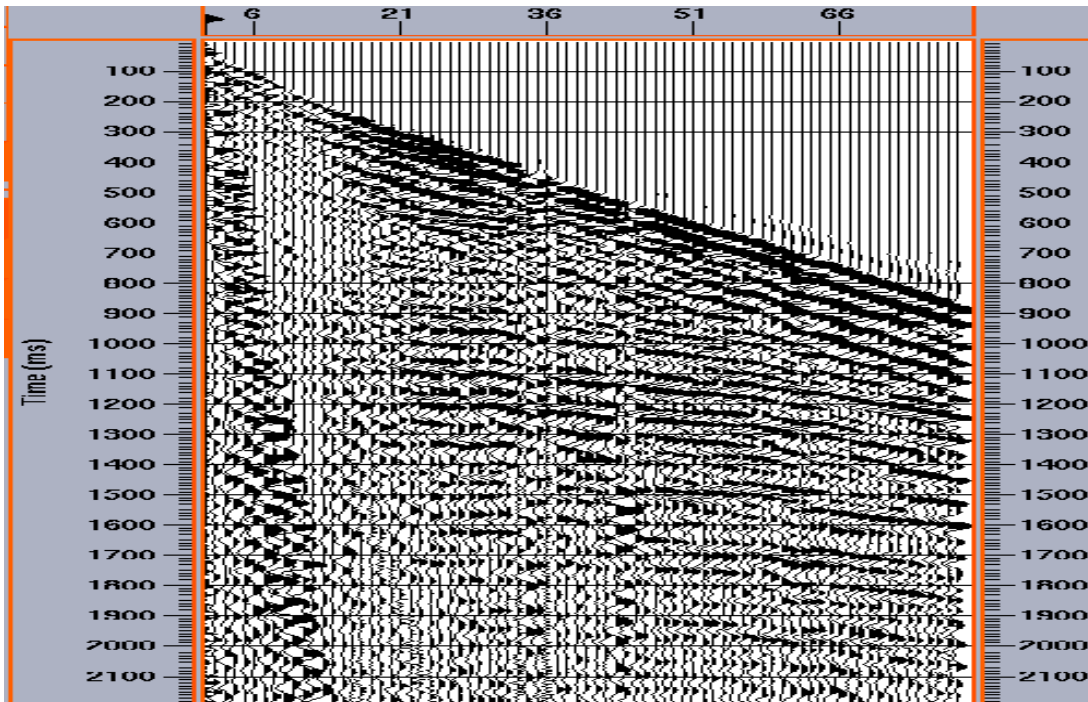


FIG. 10: Correlated shot gather for vibe point 27 m from borehole.

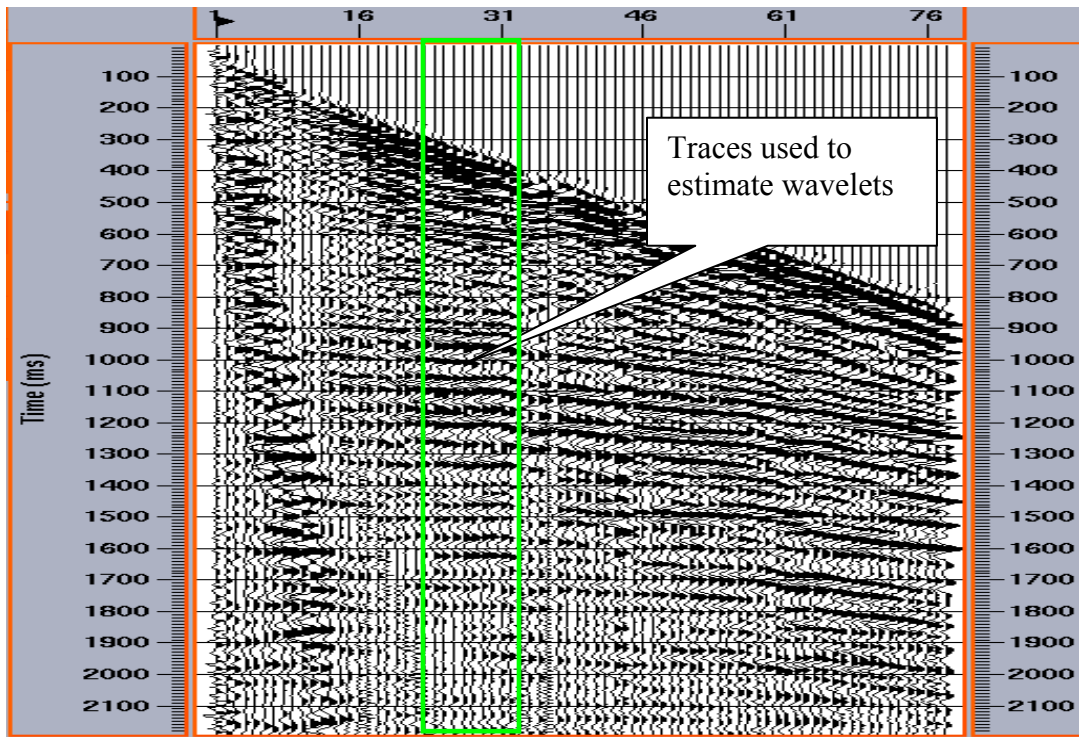


FIG. 11: Shot gather shown in Figure 9 after noise suppression.

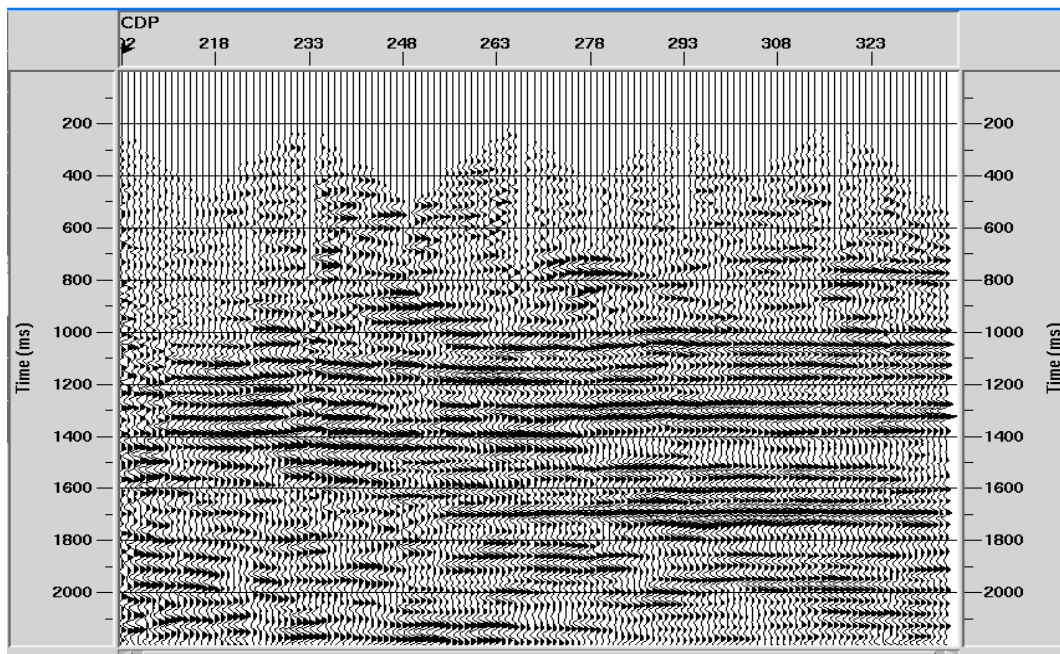


FIG. 12: Stack section.

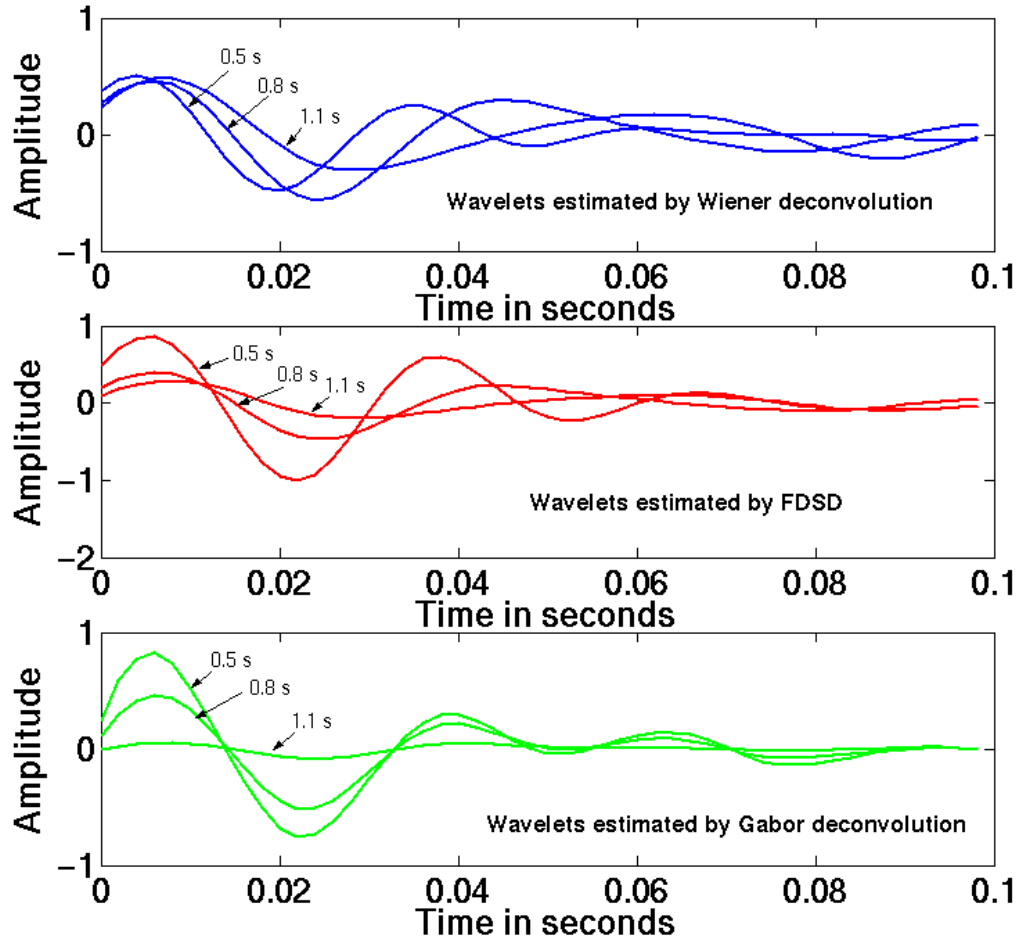


FIG. 13: Wavelets estimated by Wiener, frequency domain spiking (FDSD) and Gabor deconvolution.

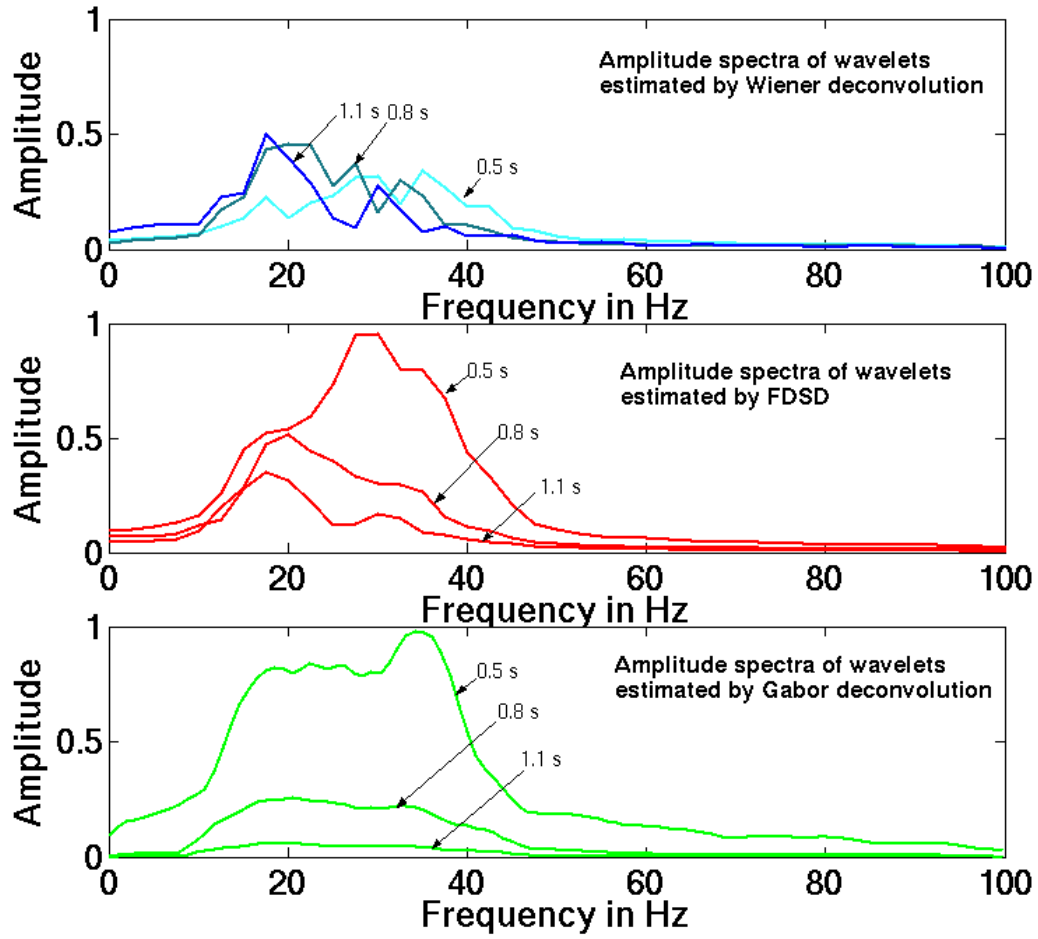


FIG. 14: Amplitude spectra of the wavelets estimated by Wiener, frequency domain spiking (FDSD) and Gabor deconvolution.

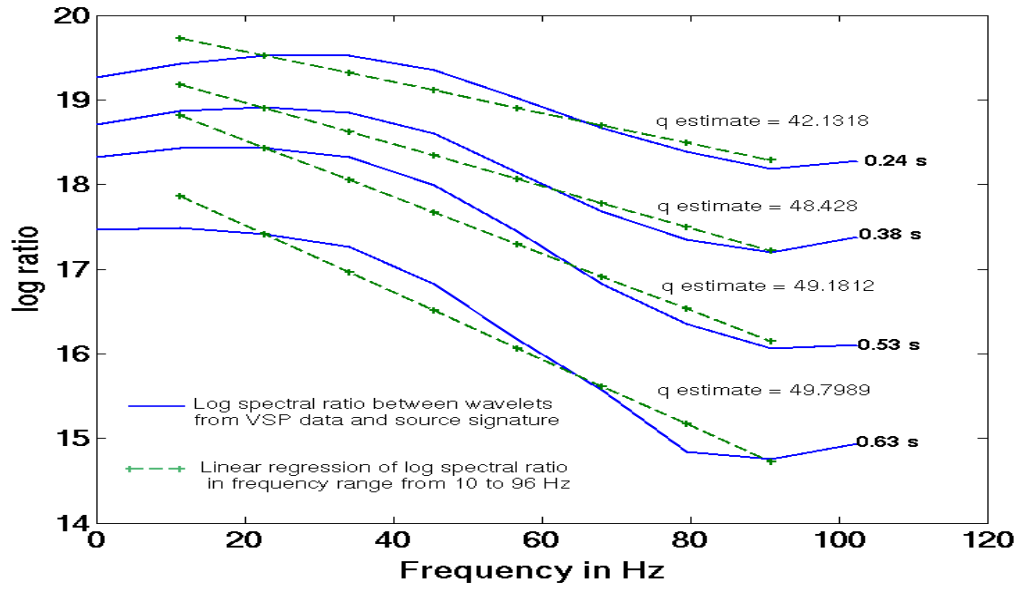


FIG. 15: Log spectral ratios calculated using Equation 5, and estimated Q values.

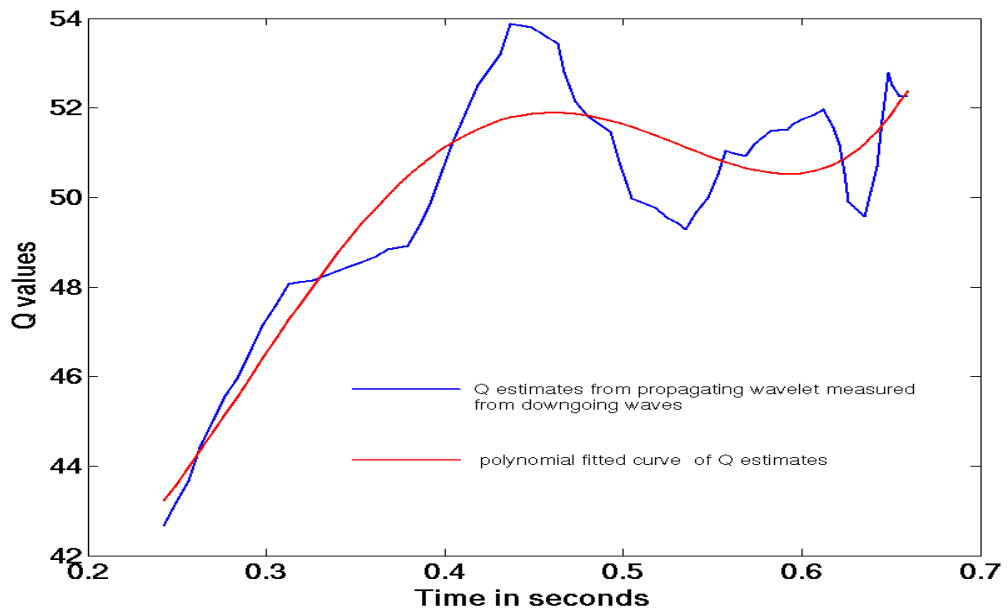


FIG. 16: Average Q values estimated by spectral ratio method from VSP downgoing waves.

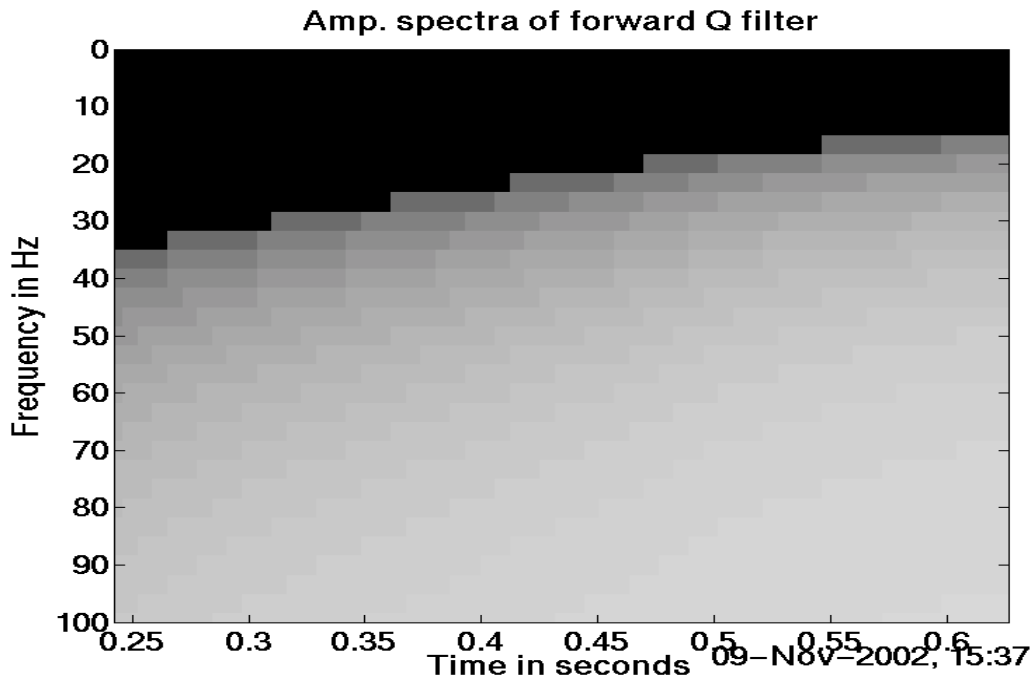


FIG. 17: Time-frequency domain forward-Q filter calculated from polynomial curve shown in Figure 16.

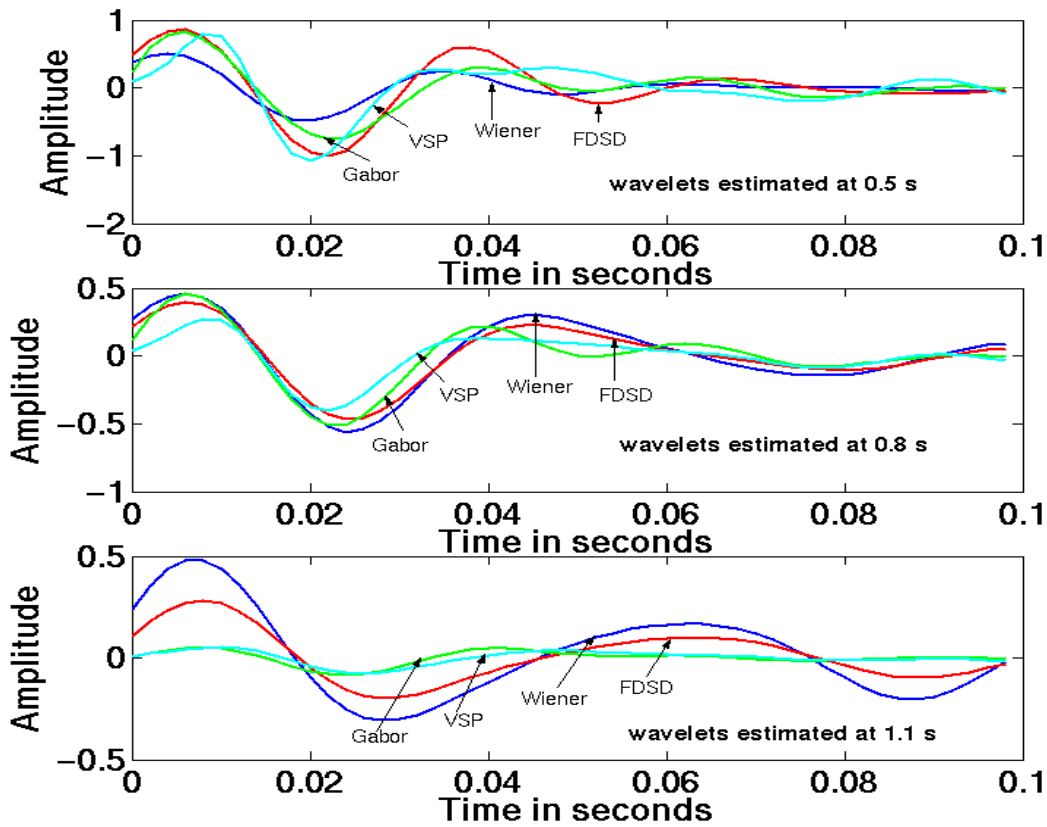


FIG. 18: Wavelets estimated from surface data by Wiener, frequency domain spiking (FDSD) and Gabor deconvolution (Figure 12), and Q-filtered wavelets estimated from VSP data.

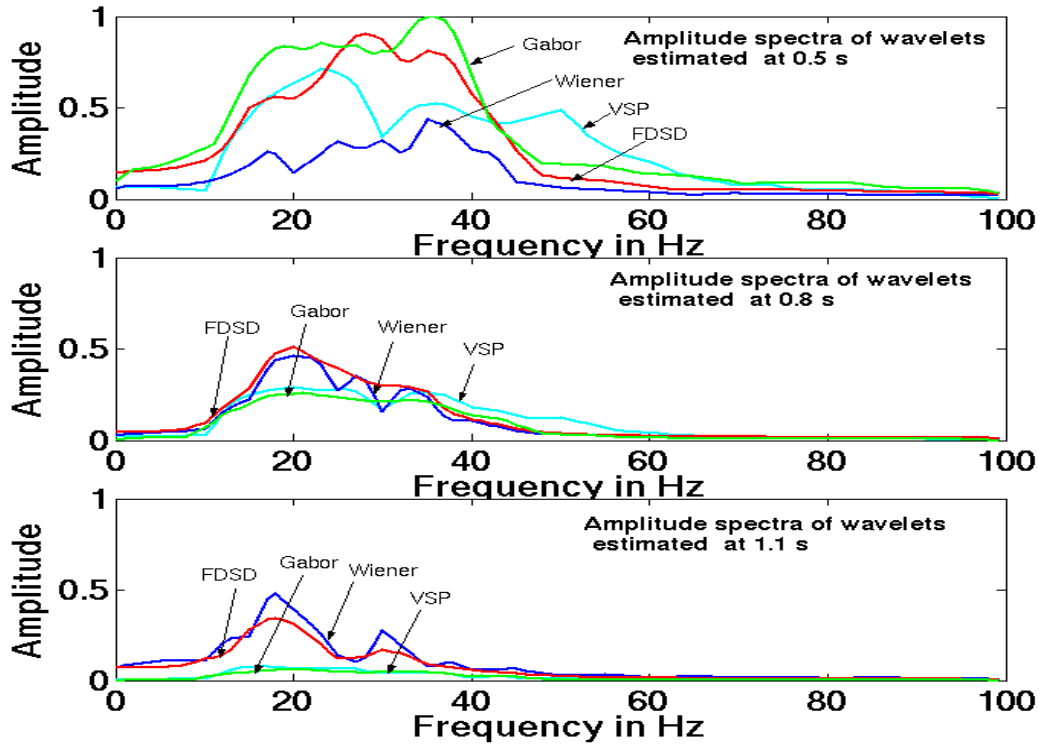


FIG. 19: Amplitude spectra of wavelets shown in Figure 17. estimated by Wiener, frequency domain spiking (FDSD) and Gabor deconvolution, and amplitude spectrum of Q-filtered wavelets from VSP data.

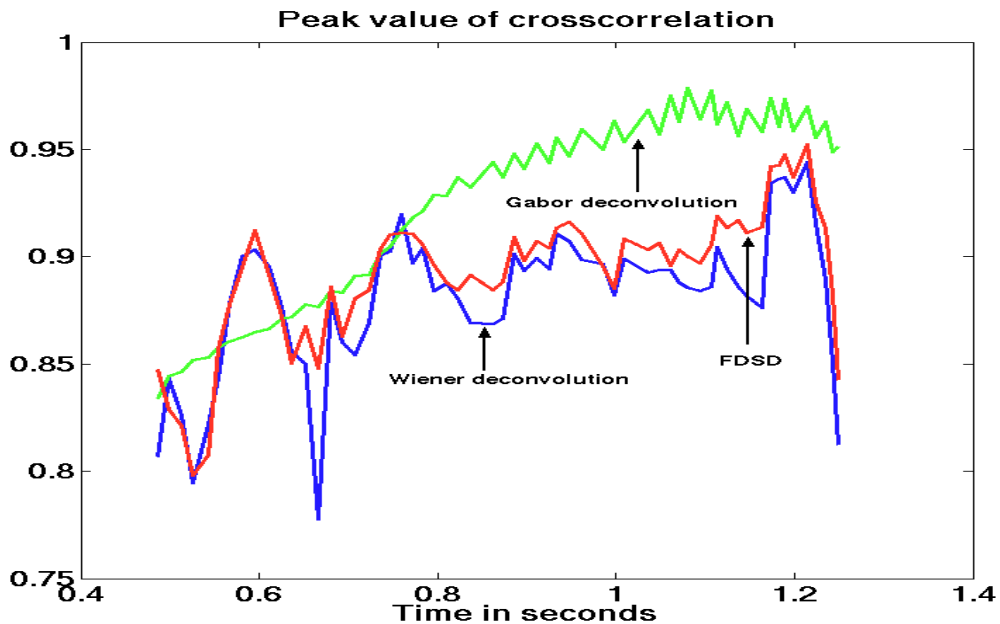


FIG. 20: Peak value of the crosscorrelation between Q-filtered wavelets from VSP and the wavelets estimated from surface data.